Solenoid gas puff imploding liner x-ray source

G. D. Lougheed, M. M. Kekez, J. H. W. Lau, and R. P. Gupta
National Research Council Canada, Ottawa K1A OR6, Canada

(Received 6 May 1988; accepted for publication 26 September 1988)

There is a worldwide effort to produce a soft x-ray source for submicron microlithography to manufacture future generation large scale integrated microchips. The gas puff plasma discharge has been suggested as a viable alternative for low volume facilities which require relatively low throughputs with a single aligner station. The repetition rate for such systems is limited by the large gas flow into the vacuum system with the standard electromechanical puff valve. A unique puff arrangement is being developed which will limit the dead gas flow and, in principle, will allow for the development of high repetition rate systems. In this arrangement, the gas flows continuously from a low-pressure plenum through an annular aperture into the Z-pinch electrode gap. A discharge through a single turn solenoid coil mounted on the outside of the plenum inductively heats the gas, temporarily increasing the mass flow to produce a low mass ($<1\ \mu$g), preionized liner which is imploded by a Z-pinch current discharge. (Multiturn coils have also been used. However, all the experiments reported in this paper used a single turn configuration.) Experiments were carried out with a variety of low-energy (<2.5 kJ) drivers including capacitor banks, peaking capacitors, and dc charged paper/castor oil Blumleins. Radiation measurements in the ultrasoft and soft x-ray regions were made using x-ray diodes, *p-i-n* diodes, and a time integrated pinhole camera. A slug model coupled to a capacitor bank or Blumlein circuit solver is used to estimate the liner dynamics as well as the load current and voltage.

I. INTRODUCTION

The microelectronics industry has evolved very rapidly in recent years, and submicron resolutions will soon be required in commercial fabrication.[1] Presently, optical lithography systems using steppers and 1:1 scanning systems are performing successfully around 1 μm. There is considerable debate regarding how far this technology can be extended into the submicron region.[1,2]

X-ray lithography was established as a viable submicron fabrication technique by Spears and Smith using an electron impact system.[3] Several alternative x-ray sources have been proposed for commercial application. These include electron impact systems, laser and discharge plasmas, and compact synchrotrons. The high brightness pulsed plasma discharge sources have been established as viable alternatives for small and moderate sized production facilities which can only economically utilize a single aligner station.[4] Several groups have shown submicron (0.5 μm) replication in laboratory tests.[5]

Several plasma discharge systems have been suggested for producing high brightness radiation sources for microlithography and other applications. Most of these devices (the gas puff,[5] plasma focus,[6] and hypocycloidal pinch[7]) are variations of the Z-pinch geometry. In Z-pinch devices, a high current is produced on the outer edge of a cylindrical volume of gas using a pulsed electrical driver such as a fast capacitor bank. The resulting $\mathbf{J}\times\mathbf{B}$ force accelerates the plasma shell radially inward to form a very high-temperature plasma on-axis which emits characteristic thermal radiation in the soft x-ray region.

Z-pinch implosions of hollow shell liners derived from foils,[8] wire arrays,[9] and gas puff systems[10] have been used extensively for the production of pulsed high fluence laboratory sources of soft x rays (>1 keV).

The gas puff Z-pinch systems have been studied extensively as possible sources for x-ray microlithography. The problems which may limit the commercial application of these systems are as follows: (1) high gas throughput into the chamber, which will limit repetition rate; (2) uniform gas preionization, which would allow efficient, stable operation with a large initial radius, low density shell is difficult; (3) limited to use of high Z gases with only the krypton l-shell lines giving an optimum match to microlithography requirements.

We have suggested two alternate methods, the multiple vacuum arc and solenoid gas puff, for producing the initial gas shell for the Z-pinch system. In both cases, the material is injected into the interelectrode gap as a plasma, thus minimizing preionization problems and allowing the use of low mass large initial radius systems with high-energy coupling efficiency. The mass injected into the chamber is minimized, thus allowing, in principle, the development of a high repetition rate system. The multiple vacuum arc system has the additional advantage of producing the hydrogen- and heliumlike lines from lower Z elements, such as aluminum or magnesium, which give a good match to microlithography requirements and can be produced more efficiently than the krypton l-shell lines. This system has not been as well developed as the solenoid gas puff system, and only the latter system will be discussed in detail.

II. MICROLITHOGRAPHY SYSTEM REQUIREMENTS

A plasma discharge soft x-ray suitable for microlithography must meet several basic requirements. For wafer rep-

 0021-8979/89/030978-15$02.40

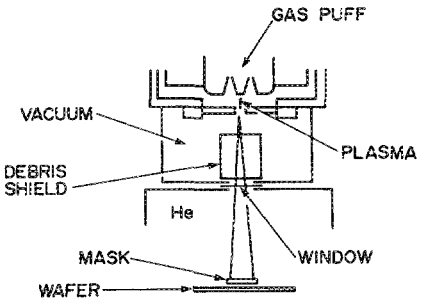

FIG. 1. The microlithography geometry with a gas puff soft x-ray source.

lication, a point source of radiation is used to proximity focus a mask onto the wafer which is coated with a photoresist (Fig. 1). The Fresnel diffraction-limited line resolution is given by[11]

$$\delta_F = 0.4[\lambda(S/2)]^{1/2}, \tag{1}$$

which is approximately 0.1 μm for $\lambda = 1$ nm and a 20-μm mask-wafer separation. This is of the same order as the penumbral blurring given by

$$\delta_P = Sd/D, \tag{2}$$

where S and D are the mask-wafer and the mask-source separations and d is the source diameter.

Thermal loading on the mask is a particular problem associated with pulsed plasma sources which emit intense radiation (10^5–10^6 W) for tens of ns. The mask is cooled by conduction through the helium atmosphere on a ms time scale. The residual mask temperature should have a minimum effect for sources with repetition rates up to several hundred Hz. The difference in the thermal expansion coefficient of the gold absorber and the thin, transparent substrate can result in high stress and strain at the interfacial bond with the potential of producing delamination either from a single high-energy pulse or long-term fatigue. Calculations indicate a flux limit of 15 mJ/cm^2 for shear/fatigue problems.[12] Mask distortion or buckling with the thermal loading must also be minimized. Calculations indicate that the membranes can be sufficiently prestressed to keep the maximum distortion in acceptable limits for temperature increases of 60 °C, provided the mask is uniformly irradiated and the gold coverage is equally distributed over the mask area.[13]

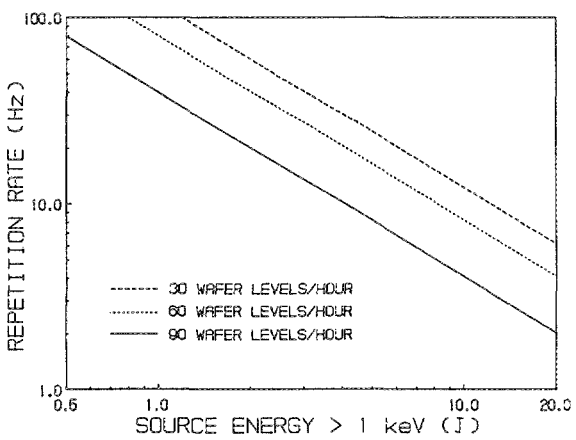

FIG. 2. The wafer throughput for repetitive soft x-ray sources assuming 0.15-μm source-to-wafer distance, six subfields/wafers, a 100-mJ/cm^2 resist sensitivity, and e^{-1} losses in the window and mask substrate.

TABLE I. Lithography source requirements.

Parameter	Required
Size	< 1 mm
Source-to-wafer distance	15 cm
X-ray energy	1–3 keV
Energy/pulse	1–5 J
Maximum dosage on wafer	1–5 mJ/cm^2
Repetition rate	1–100 Hz
Peak current	400–500 kA
Current rise	1–2 TA/s
Position reproducibility	< 1 mm
Reliability	10^6–10^8 shots

Mask damage, due to single shot effects as well as cumulative effects, limits the output of high brightness pulsed sources which can be utilized for microlithography. High throughput is obtained using a fast repetition system. Estimated throughputs are shown in Fig. 2 in terms of repetition rate and source output assuming a 100-mJ/cm^2 resist sensitivity, six subfields/wafer, and e^{-1} transmission through the vacuum window and the mask substrate for the geometry given in Table I. Mask damage would become a problem for radiation sources in the 30-J range.

The shot-to-shot variation in the radiation output must also be considered when determining operating parameters. A higher repetition rate/lower energy system would allow for statistical averaging to minimize variation in the resist dosage.

Several other factors must be considered in the development of a radiation source suitable for microlithography. These include high component reliability, minimal shot-to-shot variation in source position and output energy, high-energy coupling efficiency to radiation in 1.5–2.0-keV range to minimize window attenuation, and total power consumption.

III. SOLENOID GAS PUFF SYSTEM

Conventional gas puff systems use a magnetically driven mechanical valve to control the flow of high-pressure (few atmospheres) gas into a high velocity annular nozzle in one of the Z-pinch electrodes.[14] These systems require relatively long opening and closing time of several ms, thus allowing considerable gas flow into the chamber which must be pumped out between shots. Only neutral gas is injected into the chamber, and efficient preionization is required to minimize initial perturbations due to long current formation times.[15]

In the solenoid gas puff system,[16] the gas is allowed to flow continuously from a plenum into the Z-pinch diode gap through a narrow slit, or an annular array of capillaries (Fig. 3). The pressure in the main vacuum chamber is maintained at less than 1 mTorr by a high capacity vacuum pump for 0.1–10-Torr plenum pressures. A pulsed discharge through a single turn coil mounted on the outside of the gas plenum produces a current in the low-pressure gas producing rapid

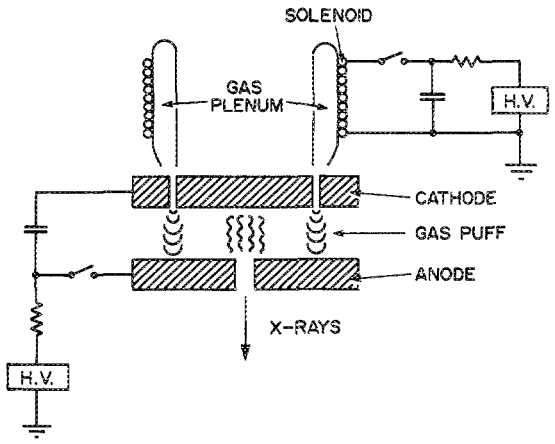

FIG. 3. A sketch of the solenoid gas puff arrangement.

heating and, as a result of the increased gas pressure and magnetic pressure, the mass flow rate into the diode during the discharge period. The resulting plasma annulus is imploded by the current produced by the primary Z-pinch discharge. Multiturn coils have also been used. However, all the results reported in this paper utilized a single turn system.

A 500-ℓ/s turbomolecular pump is used to maintain the chamber in the 0.1–1.0-mTorr range under steady flow conditions. The maximum gas throughput is 0.5-Torr ℓ/s assuming

$$Q = pS, \tag{3}$$

where p is the pressure in Torr and S is the pumping speed in ℓ/s.[17] For krypton, this gives a maximum mass throughput of 2.5 mg/s.

The mass flow for choked continuum flow of an ideal gas is given by[18]

$$\dot{m} = \rho_0 a_0 A (2/\gamma + 1)^{(\gamma+1)/2(\gamma-1)}, \tag{4}$$

where ρ_0 and a_0 are the gas density and sound speed of the gas in the plenum, A is the nozzle area, and the specific-heat ratio γ is 5/3 for a monoatomic gas. The initial gas puff arrangement had a 25-μm annular opening on a 76 mm diam. The mass flow estimated using Eq. (4) is 28.6 mg/s. The nozzle has a relatively large length/opening cross-section ratio with the result that wall and viscous effects will reduce the mass flow rate.

A 2.8-μF capacitor charged to 20 kV is used to drive a current through a single turn coil. The discharge has a 8-μs period and 70-kA peak current. The azimuthal electric field induced in the low-pressure gas plenum is sufficient to break down the gas and the resulting plasma current heats the gas. Assuming the gas can be heated to 3 eV, the gas sound speed will be increased by ten times, and using Eq. (4), the mass flow rate should increase by the same ratio. The initial flow conditions noted above would suggest that the mass flow would be <25 ng/μs with low mass 0.1–0.5-μg liners formed in 10–30 μs.

The gas exiting the nozzle will have a flow velocity roughly equivalent to the sound velocity in the plenum. For krypton with an initial sound speed of 240 m/s, approximately 4 μs is required for the flow to transit the 10-mm electrode gap and 5-mm nozzle.

TABLE II. Gas puff configurations.

Gas puff geometry	Number of openings	Opening size (μm)	Initial radius (mm)
Annulus	1	25.4	38.8
Annulus	1	38.1	38.8
Capillaries	10	381.0	35.0
Capillaries	10	508.0	35.0
Capillaries	10	635.0	35.0
Capillaries	8	342.9	32.0
Capillaries	8	406.4	32.0
Capillaries	16	406.4	32.0
Capillaries	32	406.4	32.0

Both annular and capillary systems have been used with the various configurations summarized in Table II. The initial pressure conditions in the chamber and the plenum for krypton are shown in Fig. 4 for annular openings and Fig. 5 for the capillary systems. The plenum pressures are measured using a capacitive gauge head with a 0.01–1000-Torr range. The chamber pressures are measured with both UHV ion and cold cathode gauges. A scaling factor of 1.9 is required for krypton to adjust the gauge reading to give the chamber pressure.[19]

IV. EXPERIMENTAL ARRANGEMENT

The initial experiments were carried out with the arrangement shown in Fig. 6(a). The insulator used to isolate the two electrodes was also used to form a 100-mm-diam vacuum section. The base of the chamber was machined to allow access for a 50-mm-wide high voltage transmission line which was connected to an aluminum disk electrode. The solenoid gas puff system was mounted on a disk which formed the top of the chamber as well as the ground electrode. A screen assembly on the outside of the vacuum chamber was used to connect the ground electrode to the parallel plate transmission line. A 50-mm aperture through the center of the puff assembly was used for both diagnostic and vacuum access. Preliminary results regarding the feasibility of the solenoid gas puff concept were obtained with this arrangement. These results are summarized in Sec. VI.

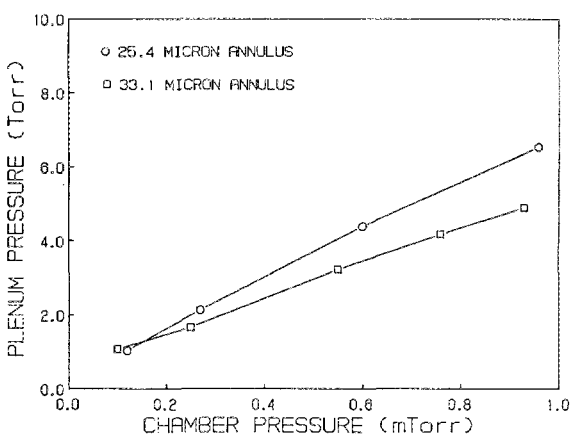

FIG. 4. The initial gas flow conditions using the 76-mm-diam annular puff arrangement.

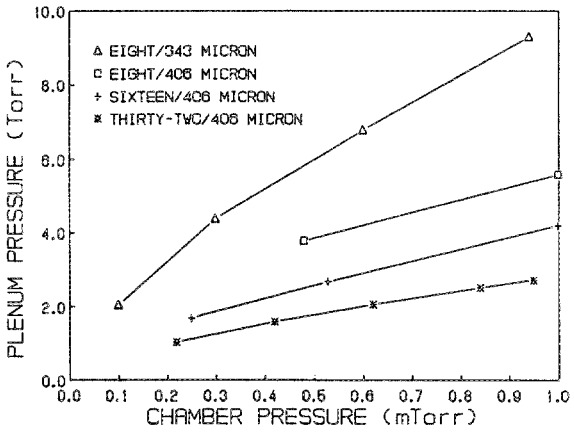

FIG. 5. The initial gas flow conditions using the capillary puff systems with the capillaries located on a 64 mm diam.

A low inductance (10 nH) central load and vacuum feedthrough section, Fig. 6(b), has been used for the majority of the experiments. The four sides of the 0.5-m square load section are accessible for attaching capacitor banks. The Mylar insulation blankets are overlapped to maintain insulation integrity. The vacuum transmission section is shaped to minimize radiation illumination of the insulator. The gas puff arrangement is mounted on the high voltage electrode with the solenoid coil encapsulated in epoxy for electrical isolation. A 0.2-m-i.d. cylindrical vacuum chamber is mounted on the ground plate. The vacuum pump is mounted in the direct line of sight of the electrode region to maximize conductance. Diagnostic ports at 33° and 45° to the central axis view the central pinch region. This arrangement gives good diagnostic and vacuum pumping access to the diode region, as well as a low inductance load and feedthrough section to maximize energy coupling to the load.

Various pulsed power drivers have been used to produce the current for the Z-pinch implosions. The electrical characteristics for these systems are briefly summarized in Table III. Several capacitor bank systems were used in the initial phases of the experimental study while the fast pulse Blumlein systems were being developed. Some experiments were carried out with peaking capacitor systems in an attempt to increase the current rise. However, various Blumlein configurations were used for the majority of the experiments. The results using the capacitor banks and the peaking circuits are briefly summarized for completeness.

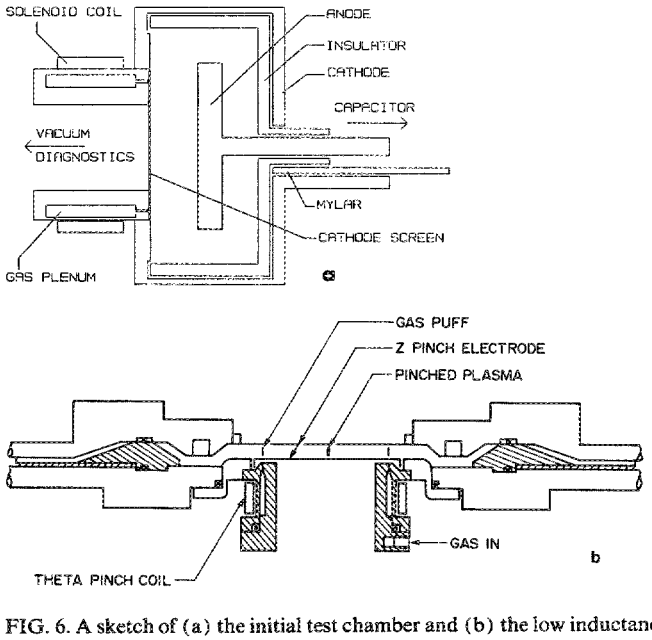

FIG. 6. A sketch of (a) the initial test chamber and (b) the low inductance electrode and gas puff arrangement.

TABLE III. Capacitor banks.

Configuration	C (μF)	V (kV)	I (kA)	$\tau_{1/4}$ (ns)	Energy (kJ)
Capacitor	1.8	20	84.9	730.0	0.36
Capacitor	2.8	20	105.8	831.8	0.56
Capacitor	5.6	20–30	302.7	871.8	2.52
Peaking	2.8/2.8	20	125.0	600.0	0.56
Peaking	5.6/1.8	20	191.9	750.0	1.12
Peaking	5.6/8×0.22	20	300.0	700.0	1.12
Blumlein	1.8	25	190.0	320.0	0.56
Blumlein	3.7	25	290.0	320.0	1.16
Blumlein	5.6	25	480.0	360.0	1.73

Peaking capacitor circuits have been used extensively in pulsed power transmission lines to maximize peak current and current rise time. Systems utilizing standard capacitor banks with peaking circuits have been used to drive UV and laser sources.[20,21] A secondary switch (or the load acting as a switch) is used to maximize energy transfer to the peaking capacitor before current initiation in the load. In the Z-pinch experiments, a secondary switch was not incorporated in the circuit (Fig. 7), and any switching action was provided by the load.

Simulations have been carried out using the University of Waterloo WATAND circuit code.[22] Results for a 5.6-μF capacitor bank driving a 1.6-μF peaking capacitor and a 3-nH, 20-mΩ load are shown in Fig. 8. There is an increase in peak current and rise time even for the zero delay situation illustrated in Fig. 8(b). There is a further enhancement of current parameters if the load acts as a switch and delays the current initiation in the load. For higher inductance peaking capacitor circuits, 300–500-ns delays are required to maximize the effect whereas shorter delays can be tolerated for the lower inductance systems.

Small dc charged Blumlein systems using both coaxial and stripline construction have been used to produce the short current pulses required for N_2 laser pumping as well as for flash x-ray sources.[23,24] Relatively low energies (<100 J) have been used to drive short duration pulses with <15-kA peak currents. A Blumlein system which extends the

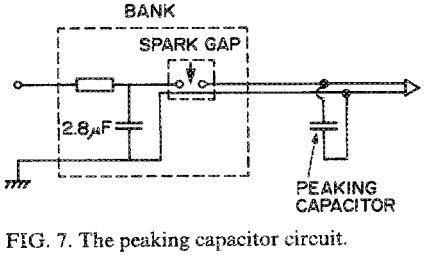

FIG. 7. The peaking capacitor circuit.

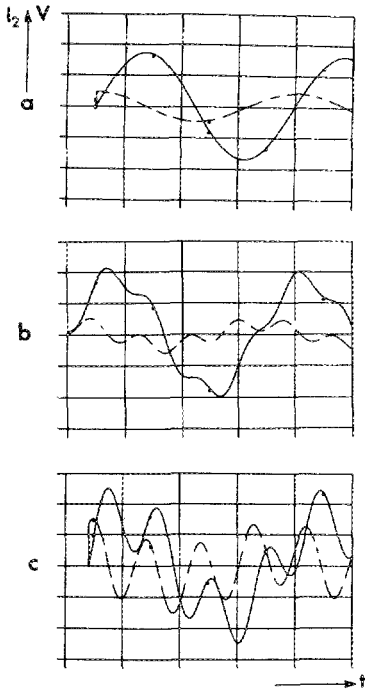

FIG. 8. Simulated currents (solid line) and voltages (broken line) with 200 kA/div and 20 kV/div, respectively, and 1 μs/div for a 5.6-μF, 20-kV, and 40-nH capacitor bank with a 3-nH load inductance and 20-mΩ load resistance for (a) no peaking capacitor, (b) 1.6-μF peaking capacitor with no delay, and (c) 1.6-μF peaking capacitor with 300-ns delay.

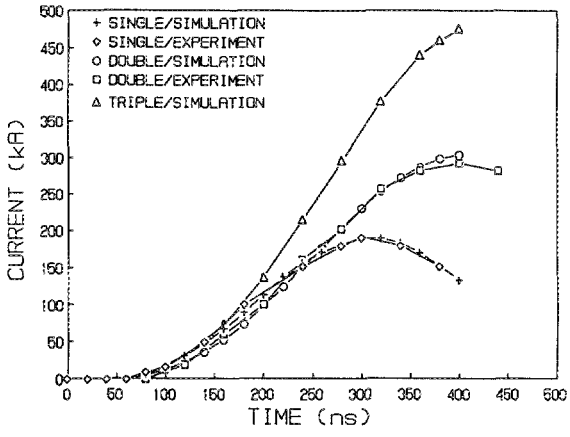

FIG. 9. Experimental and simulated short-circuit currents for the dual single, dual double, and triple Blumlein configurations.

energy and current parameters to the range of interest for Z-pinch implosions has been developed.[25] A strip line configuration with a laminated electrical grade kraft paper dielectric blanket and layered commercial aluminum foil conductors is used to minimize the impedance. Both single and double line configurations have been constructed. The electrical characteristics for the Blumlein combinations used for the Z-pinch implosions are summarized in Table IV.

A Blumlein circuit model has been developed assuming two transmission lines connected across the load represented by an initial parasitic inductance.[26] The model is described in detail in Ref. 25. The circuit model has been used to simulate the short-circuit currents for the three Blumlein combinations which have been utilized [dual singles, two doubles, as well as two singles and dual doubles (triple) modules in parallel]. A composite model is assumed for each combination with electrical parameters given by adding together the appropriate single module parameters. The results for the three line combinations are shown in Fig. 9 along with experimental results for the two single and double configurations. The lines are dc charged to 25 kV. A 10-nH parasitic load and 24-nH/switch inductances are assumed. The switch inductance is 20% higher than stated by the manufacturer.[27] However, the units were used at voltages well below the minimum operating range (50–100 kV) and, as a result, full multichanneling may not be obtained.

Peak short-circuit currents of 190, 280, and 500 kA with 125-, 150-, and 200-ns rise times (10%–90%) were obtained with the dual singles, dual double, and triple Blumlein combinations. Both the load and switch inductances are important factors in the current parameters that can be achieved. A more compact switch element explicitly designed for the Blumlein application could greatly improve current results and thus energy coupling efficiency. It should be noted, however, that even with the present switch modules the Blumleins are very efficient current drivers with 300 kA/kJ of stored energy and current rises $> 10^{12}$ A/s.

The simultaneous triggering and discharge of the individual modules into the load is necessary to ensure maximum current. The switches are triggered with a Maxwell 100-kV generator.[28] Current probes placed in the parallel plate feeds from the individual Blumlein modules have been used to ensure the switch electrodes are optimally adjusted.

A Rogowski coil is mounted in the vacuum section of the return conductor just outside the initial plasma diameter [see Fig. 6(b)]. A 100-kV fast transient (5 ns) voltage probe connected to the conductors external to the chamber has been used for voltage measurements. Aluminum photocathode XRDs filtered with 1.5-μm Mylar, 4.0-μm kimfoil, and 12.5-μm saran have been used for measurements at 150–288 eV using the carbon k-edge and 1.5–2.8 keV using the chlorine k-edge. p-i-n diodes with 12.5- and 25-μm Be filters as well as 6.0-, 12.0-, and 25.0-μm aluminum filters have been used to measure radiation in the 1.0–15.0-keV range. An x-ray pinhole camera which can give three separate images on Kodak RAR 2495 or DEF film has been used with 12.5- and 25.4-μm Be filters and a 25-μm Al filter to produce pictures of the soft x-ray emitting region. An aluminized kimfoil is also available for exposures in the ultrasoft x-ray region (> 500 eV).

TABLE IV. Electrical characteristics oil/paper Blumleins.

Configuration	C_1 (μF/m)	L_1 (nH/m)	Z_0 (mΩ)	C (μF)	Energy[a] (J)	Size (m^3)
Single	0.06	1.05	0.128	0.9	272	0.038
Double	0.13	0.50	0.062	1.8	544	0.058
Dual singles	0.13	0.50	0.062	1.8	544	
Dual doubles	0.25	0.26	0.032	3.5	1087	
Triple[b]	0.38	0.17	0.021	5.3	1632	

[a] Energies estimated assuming the lines are dc charged to 25 kV.
[b] Two singles and two doubles combined.

V. SLUG MODEL

Zero-dimensional models have been used extensively to analyze the dynamics of various liner implosions.[29] The

equation of motion for a thin shell plasma accelerated by the magnetic pressure produced by a Z-pinch discharge current is given by

$$F = -(m\mu_0 I^2/4\pi r), \tag{5}$$

where m is the mass in kg/m, r is the radius in m, and I is the current in A. A capacitor bank or the Blumlein circuit model is used to determine the time-dependent current which can be coupled to Eq. (5). Results of these calculations are discussed along with the experimental results in the next section.

The equation of motion can be solved numerically if the current is linearly proportional to time, and is given by

$$I = At, \tag{6}$$

with A in A/s.[30] Relations for the implosion time t, liner kinetic energy KE, and ion kinetic energy $\mathrm{KE_{ion}}$ can be derived, and are given by

$$t = 95.6(R_0/A)m^{1/4}, \tag{7}$$

$$\mathrm{KE} = 1.9\times 10^{-3}(At)^2, \tag{8}$$

$$\mathrm{KE_{ion}} = 2.16\times 10^{-7}Z^{1.15}(A/t)^2, \tag{9}$$

where R_0 is the initial radius in m, Z is the atomic number for the gas, and m is the liner mass in kg. The derivation of these relations assumes an implosion to 10% of the initial radius which has been shown to be a realistic condition.[31] The implosion time, kinetic energy, and ion kinetic energy derived using these relations are shown in Figs. 10–12, respectively, for slow ($A < 1$ TA/s) and fast ($A > 1$ TA/s) current rise conditions. The former represent conditions which can be achieved with the capacitor bank discharges, and the latter the conditions for the Blumleins.

Low mass ($< 1.0\,\mu$m) liners were assumed in designing the initial solenoid gas puff arrangement. A large initial radius (76 mm) was utilized to give sufficient implosion time to allow the bank energy to be efficiently coupled to the liner. With the slower capacitor banks, only the initial 300–500 ns of the current pulse can be utilized. The energy delivered during the remainder of the current pulse (see Fig. 13) is not utilized. The Blumleins were developed to give a faster current rise and increase energy coupling to the dynamic load.

There are inherent problems with large initial diameter implosions. Experiments with other imploding liner configurations[32] indicate that Rayleigh–Taylor instabilities may result in plasma shell broadening or break up, and thus lead to a low-temperature large radius pinch phase. However, high ion kinetic energy can be achieved with the large initial radius implosions.

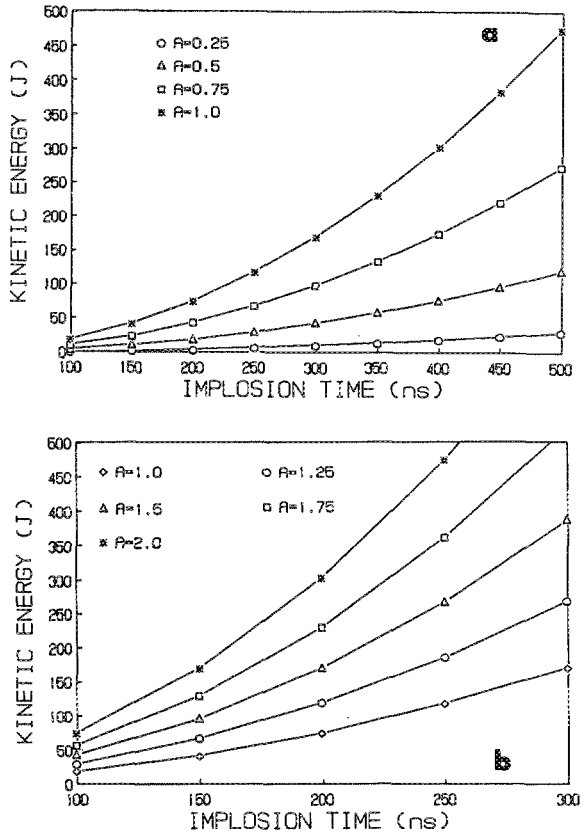

FIG. 11. The kinetic energy coupled to the dynamic load with current rises of (a) 0.25–1.0 TA/s and (b) 1.0–2.0 TA/s.

VI. EXPERIMENTAL RESULTS

The solenoid gas puff research program was initiated to determine (a) the scientific feasibility of using the concept to produce gas/plasma liners for fast Z-pinch implosions, and (b) if a soft x-ray source with suitable parameters for x-ray

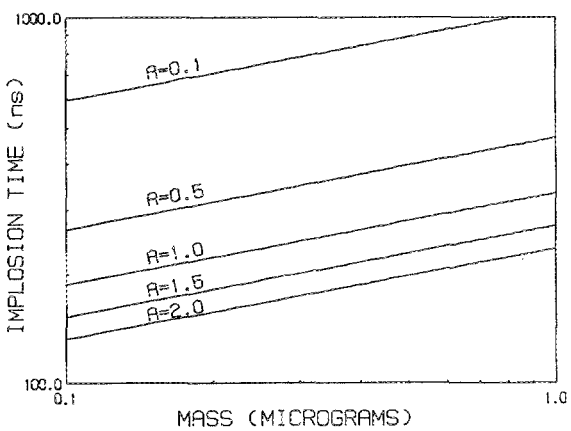

FIG. 10. The implosion times for the large radius puff for current rises in the 0.1–2.0-TA/s range.

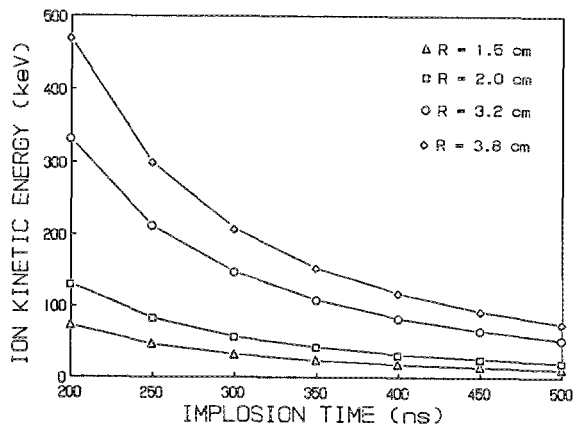

FIG. 12. The ion kinetic energy with 15-, 20-, 32-, and 38-mm initial puff radius.

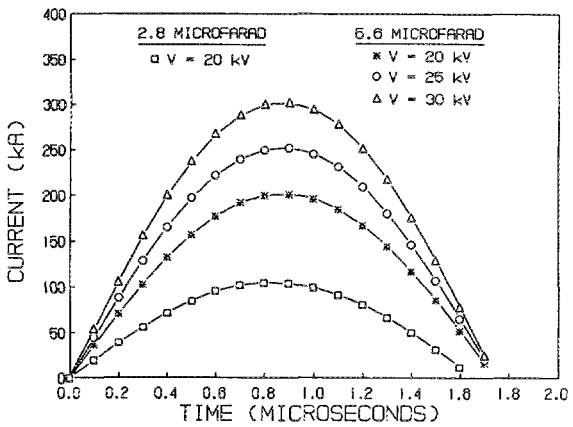

FIG. 13. The capacitor bank current waveforms.

microlithography could be realized on a single shot basis. As was noted in Sec. IV, a variety of drivers, vacuum arrangements, and gas puff configurations have been used at various stages in the program. The initial studies were carried out with existing low inductance capacitor banks and initial vacuum chamber arrangement, while the low inductance load arrangement and the fast rise time dc charged Blumlein system were developed. The majority of the experiments reported have utilized the 76-mm-diam configuration with 25- and 38-μm annular slits machined in a macor[33] plenum with $\pm$ 10% accuracy. The initial experiments were carried out using glass capillaries joined to a glass plenum. Subsequent experiments were done using a series of annular holes drilled in a macor disk and epoxied to a glass plenum.

The results for the various stages of the experimental program are summarized in this section with emphasis on the determination of operating parameters. Krypton was used throughout the program, and the radiation measurements have primarily centered on the measurement of soft radiation below the carbon k-edge using a Mylar filter and the krypton l-shell radiation using the chlorine k-edge saran filter. Some experiments were also carried out with neon, argon, and xenon.

A. Capacitor banks

The initial experiments used a 2.8-μf single capacitor bank driver coupled to the high inductance chamber [Fig. 6(b)]. Framing camera sequences with 500-ns interframe intervals are shown in Fig. 14 for a ten-capillary configuration. The initial formation and subsequent small diameter pinch can be observed in the krypton and argon implosions, but not in the neon sequence. There has been limited success throughout the program in obtaining tight pinch formations with neon. The high sound speed with the lighter gas may result in the formation of a less well-defined more diffuse liner which is difficult to break down with the second stage discharge, and as a result, will be more susceptible to instability development.

Framing camera sequences are shown in Fig. 14 for the 25-μm slit annular puff arrangement with argon [Fig. 14(d)] and krypton [Fig. 14(e)] loads. The camera monitor signal superimposed on the dI/dt trace is also shown for the latter. The visible radiation emission measured with a p-i-n diode, and the current measured with the Rogowski coil are shown along with a 2-μs streak photograph in Fig. 14(f). The implosions occur in 500–700 ns followed by an extended period of radiation. Efforts to observe the actual implosion stage have been unsuccessful in this and subsequent stages of the program with illumination from the imploding liner not visible with either the streak or framing camera.

This driver and load arrangement could only deliver 80–100 kA and 0.1 TA/s current pulses. The implosion time estimates shown in Fig. 10 would indicate a liner mass of order 0.1 μg. This high inductance system was not expected to produce much ultrasoft x rays. Measurements with a Mylar filtered XRD did indicate some emission above 100 eV.

The annular puff arrangement was subsequently utilized with the lower inductance chamber arrangement [Fig. 6(b)], and a 5.6-μF bank which could produce current pulses with 0.3–0.5-TA/s current rises. The majority of the experiments were carried out at 20 kV with 1.2-kJ stored energy.

For the initial experiments, 75% transparent screens were used as the central section for both electrodes. A 10-mm annular strip was attached to the electrode opposite the puff device to stagnate the high-speed gas flow. Pinches with implosion times up to 500 ns could be obtained. However, relatively high plenum pressures and long delays were required (Fig. 15). The ground electrode assembly was subsequently modified with a screen in the central 50-mm section and the region opposing the puff blocked by a solid electrode. Pinches with similar implosion times could be obtained with both lower plenum pressures and shorter delay time (Fig. 16). The radiation results were greatly improved with the latter configuration. Typical current and Mylar filtered XRD signals are shown in Fig. 17. The discharge through the solenoid coil requires 20 μs to ring down, and thus, with the shorter delay intervals, the triggering of the Z-pinch discharge occurs while current is still flowing in the plenum. In this regime, the liner formation is continuously ionized by the mass injected into the interelectrode gap as well as the radiation from the plenum plasma. A well-preionized liner is necessary to ensure a uniform breakdown of the main current discharge, and thus ensure minimum instability amplitude during the implosion phase. The solenoid gas puff provides uniform preionization, thus allowing the utilization of relatively low density large initial radius liners.

The injected mass can be controlled by varying the plenum pressure and the delay interval to give implosion times ranging from 200 to 700 ns. However, maximum emission in the ultrasoft x-ray region was obtained for 400-ns implosion times with predominantly UV radiation produced with longer times. With short implosion times, relatively high Be filtered p-i-n diode signals were obtained even though there was minimum or no ultrasoft emission. With the high ion kinetic energy, low particle densities inherent in this regime, there may not be adequate thermalization of the plasma with most of the radiation produced by current effects in the plasma or on the electrodes.

Experiments were also carried out with the bank

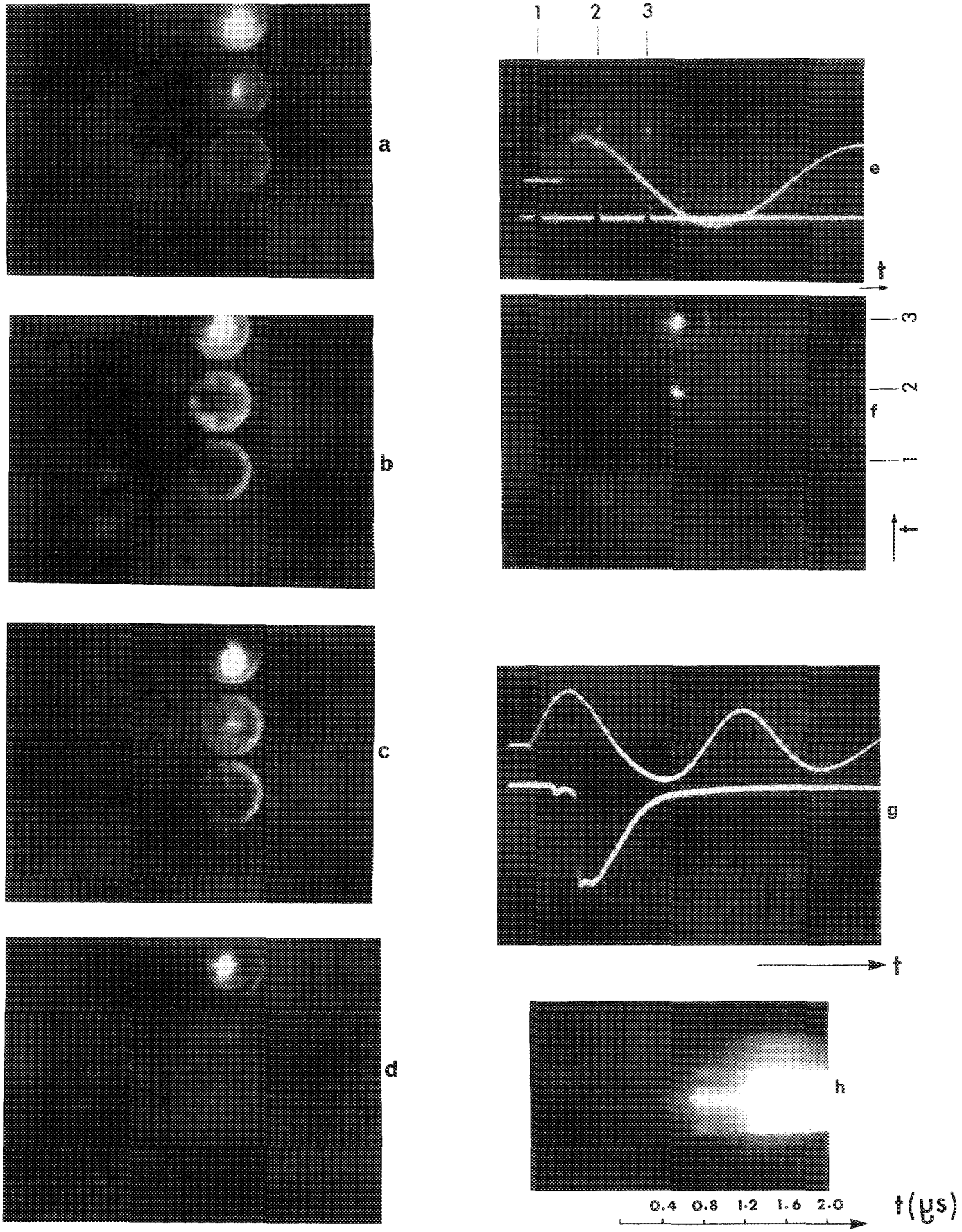

FIG. 14. Typical results with gas puff system including framing picture sequences with a 500-ns interframe interval for (a) argon, (b) neon, and (c) krypton loads with 10×381 μm capillaries, (d) argon and (e) krypton with a 25-μm annular puff, (f) the dI/dt trace and camera monitor signal (0.5 μs/div), and (g) current waveform (70 kA/div, 1 μs/div) and visible radiation measured with a light sensitive diode, and (h) 5-μs streak photograph.

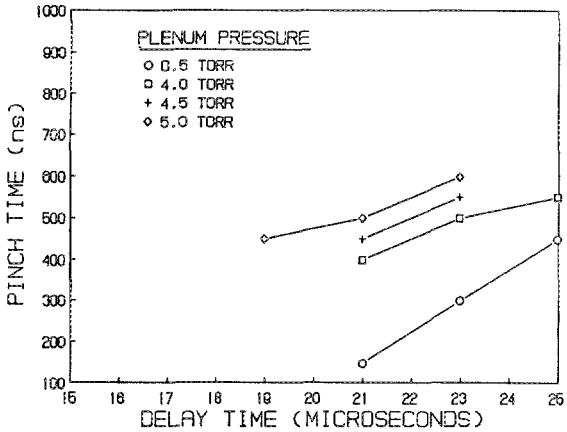

FIG. 15. The implosion time vs delay interval with a full screen on the opposing electrode.

charged to 24, 26, 28, and 30 kV. The delay/plenum pressure conditions for optimum XRD signal are shown in Fig. 18 along with similar results utilizing peaking capacitor circuits as well as Blumleins. As would be expected from the analysis in Sec. III, the rate with which mass is injected into the electrode gap is proportional to the initial cold flow rate, and thus, the initial plenum pressure. Higher plenum pressures are needed to supply the higher mass liners required for the higher current situations. Higher energy radiation is still maximized with 400-ns implosion times. The zero-dimensional calculations indicate 30–50-cm/μs velocities are required to produce the higher temperature plasmas. Substantially more radiation could be produced with the higher voltage experiments with a few joules in the ultrasoft region and 10 mJ in the soft (saran/XRD) region. These are reasonable results as only a relatively small proportion of the stored energy is coupled to the load with the slug calculations indicating 10–50 J coupled to liner kinetic energy. For the optimum 400-ns implosions, the current at pinch is limited to 175 kA. Riordan and Pearlman have shown that the soft x-ray yields for the usual gas puff devices vary approximately as I_m^4 for experiments ranging from small bench top systems to large nuclear effects simulators where I_m is the

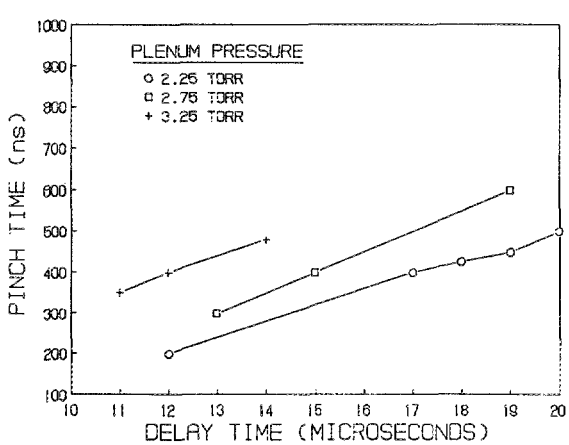

FIG. 16. The implosion time vs delay interval with a 5.0-cm-diam screen on the opposing electrode.

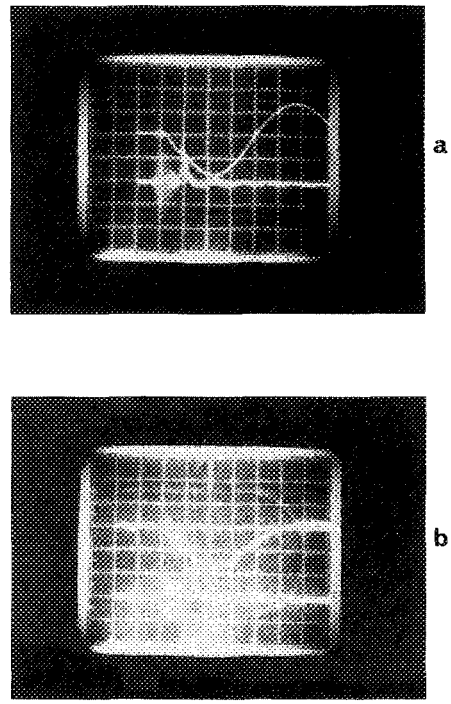

FIG. 17. The current (100 kA/div, 500 ns/div) and Mylar filtered XRD signal with 0.5 V/div with the 5.6-μF bank charged to 20 kV (a) without peaking capacitor, (b) with 1.8-μF peaking capacitor.

peak current at implosion.[4] An extrapolation to lower pinch currents using

$$Y = 75 I_m^4 \tag{10}$$

is shown in Fig. 19. Yields from some of the smaller gas puff experiments as well as the solenoid gas puff are shown. This analysis indicates that, for krypton, the l-shell emission increases rapidly above 300 kA.

B. Peaking capacitors

A peaking capacitor arrangement using a secondary 2.8-μF capacitor mounted into the transmission line between the switch and the load was tested with the initial experimental setup. The current was measured at both the initial dc charged capacitor as well as at the load. Typical

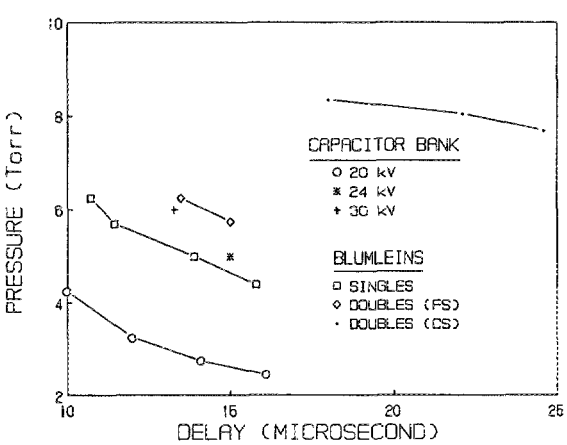

FIG. 18. The plenum pressure and delay interval operating regime for various driver configurations.

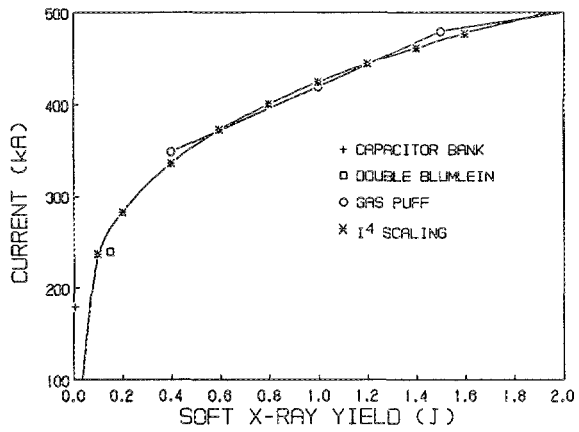

FIG. 19. The soft x-ray emission scaling with pinch current for krypton loads is shown for the solenoid gas puff system.

results are shown in Figs. 20 and 21. The *Z*-pinch diode acts as a secondary switch in this configuration with up to 1-μs delay obtained between the initial current discharge into the peaking circuit and the current initiation into the load. Both the peak current and rise are increased with up to 150 kA and 0.25-TA/s pulses obtained. There was a substantial increase in measured emission in the ultrasoft x-ray region. An XRD trace is shown in Fig. 21 along with the light diode signal with approximately 1 J now in the carbon window.

Peaking capacitors were also utilized with the low inductance load arrangement with the 5.6-μF bank charged to 20 kV. The initial tests were with a 1.8-μF, 15-nH capacitor coupled to the load section. With the low inductance load, minimum delays could be obtained between the triggering of the main switch and the current in the load, and thus only small decreases in the current rise time could be obtained. However, a factor of 3 increase in the ultrasoft radiation was measured with results comparable to those obtained with 30-kV discharges indicating a marked increase in efficiency.

Circuit analysis indicated that a further enhancement of the current parameters could be obtained even with minimal (100–200 ns) delays if the inductance of the peaking circuit is minimized. Eight Maxwell 0.2-μF, 20-nH *S*-type capacitors[34] were connected in parallel to the load and transmission lines. Typical current traces are shown in Fig. 20 along with XRD and *p-i-n* diode signals. The pulse shape is very similar to the simulation for zero delay shown in Fig. 8(b) with an initial low current leading edge and a subsequent rapid rise to 300-kA peak value at 700 ns with maximum current rises of 1 TA/s.

The radiation output shows a very strong dependence on the delay between the triggering of the gas puff and the *Z*-pinch discharge. Shorter delay intervals are required with the peaking capacitor system (Fig. 18). The secondary maximum in the radiation curve is obtained with similar delay intervals as used with the simple capacitor bank circuit.

The peaking capacitor system does enhance the radiation output when coupled with a low inductance capacitor bank to imploding liner loads by increasing both the current rise and the peak currents. However, with low inductance preionized loads it is difficult to obtain sufficient delay to maximize the effect of the peaking circuit. Without the utilization of a secondary switch, the system is very difficult to control with the jitter in the delay interval comparable to the narrow window which gives maximum radiation output.

C. Blumleins

The initial capacitor bank and peaking capacitor experiments were limited by the amount of energy which could be efficiently coupled to the dynamic load. These experiments did show, however, that the basic solenoid gas puff could

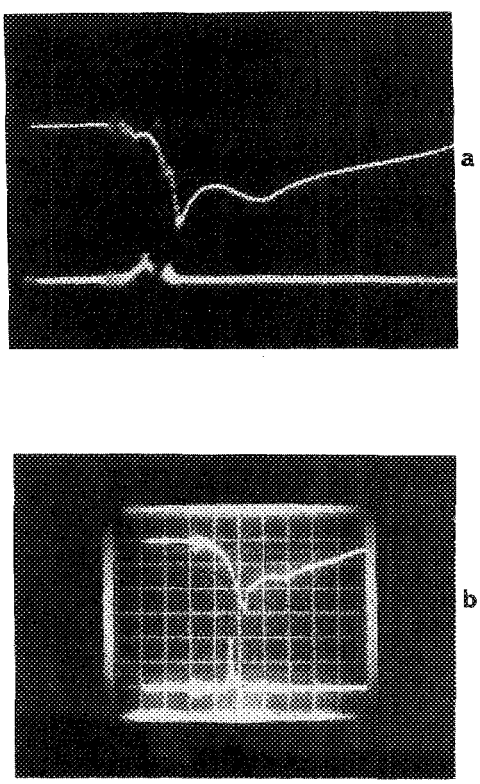

FIG. 20. Results for the 5.6-μF capacitor bank coupled with 8×0.22 μF peaking capacitors. The upper trace in each case is the current into the load with 100 kA/div and 500 ns/div and the lower traces are (a) the Mylar filtered XRD signal with 0.5 V/div, and (b) *p-i-n* diode with 12.5-μm Be filter.

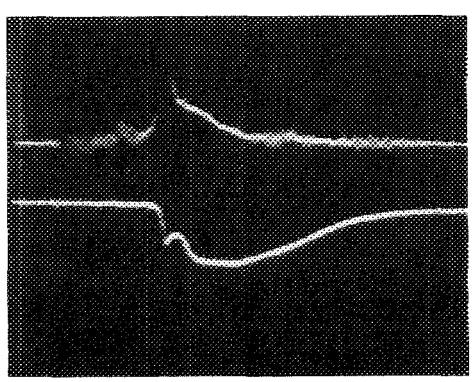

FIG. 21. The ultrasoft x-ray emission measured with the Mylar filtered XRD 2.8-μF capacitor bank and 2.8-μF peaking capacitor configuration. The lower trace is the light diode signal. The time scale is 500 ns/div.

couple low mass, large initial radius krypton liners to a Z-pinch device, and the production of ultrasoft and soft x-ray emission. The energy coupling to the liner kinetic energy, and subsequently to radiation is very dependent on both the peak current and the current rise time. The dc charged Blumleins were developed to provide the necessary current pulse. As described in Sec. IV, the Blumleins are packaged as either single or double lines connected to the same switch giving modules with 0.85 and 1.7 μF, respectively. Up to four of these modules can be connected in parallel to the central load section. Experiments have been carried out with dual single units, dual double units, as well as two singles and two doubles combined. With 25-kV operation, these three configurations give 0.55, 1.1, and 1.7 kJ of stored energy, respectively.

With the Blumleins, the current through the load is determined by the voltage pulse across the diode inductance. The high dL/dt which occurs during the final implosion phase limits the peak current which can be driven into the dynamic loads. The initial delay in the initiation of the current in the load is governed by the transit time of the voltage pulse from the switch to the load with no other inherent delays.

The peak currents (190-kA short circuit and 150 kA with load) obtained with the dual single Blumlein configurations are comparable to the capacitor bank drivers, although the rate of current rise is somewhat higher. The pressure/delay regime for optimum coupling of this configuration to radiation output is comparable to the high voltage capacitor bank results indicating similar loads are imploded. The Blumlein system, with the shorter current pulse will, however, produce high liner velocities and thus couple more energy to the liner kinetic energy with only a fraction of the stored energy.

The simulation results summarized for the dual double Blumlein system in Table V indicate that good energy coupling will be obtained with 0.2–0.5-μg liners. Initial experiments with the same diode configuration as used for both the capacitor bank and dual single Blumleins show a similar plenum pressure and delay time regime. The simulated currents assuming 0.2- and 0.3-μg loads are compared with typical experimental results in Fig. 22 using different delay intervals. Typical radiation measurements with the Mylar and saran filtered XRDs and a Be filtered p-i-n diode are shown in Fig. 23 along with a current trace. Using the nominal XRD and p-i-n diode sensitivity factors,[35,36] ultrasoft and soft radiation emissions of 1–3 J and 100 mJ are obtained.

TABLE V. Dual double Blumlein implosion dynamics.

Mass (μg)	Implosion time (ns)	Peak current (kA)	Pinch current (kA)	Velocity (m/μs)	Kinetic energy (J)	Efficiency (%)
0.1	306	175.2	163.9	1.00	50.0	4.3
0.2	340	208.6	190.3	0.81	75.7	6.5
0.3	364	226.2	201.5	0.72	78.0	6.7
0.4	384	237.5	209.9	0.64	82.2	7.1
0.5	400	245.5	212.6	0.60	88.8	7.7

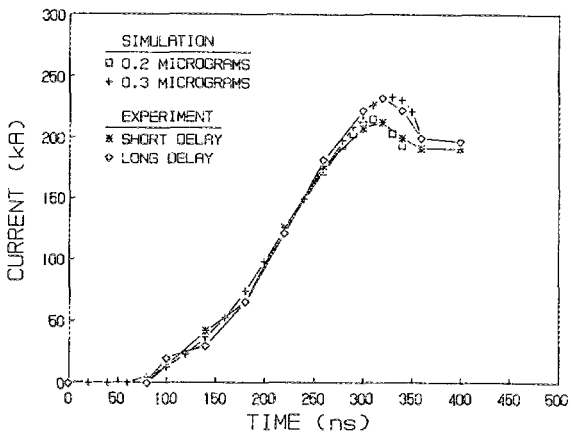

FIG. 22. Experimental and simulated currents for the dual double Blumlein configuration with krypton gas loads.

The I_m^4 scaling for the radiation output gives a comparable estimate for the pinch currents obtained (Fig. 19). These results, along those previously presented for the capacitor bank and dual single Blumlein configurations, show that the ultrafast Z-pinch x-ray sources can be extended to lower peak current regimes. For krypton, the energy conversion to soft x-ray decreases rapidly for currents less than 300 kA, suggesting that very efficient drivers would be required if a system is to be operated efficiently in this regime. With the present double Blumlein arrangement, coupling efficiencies of 0.01% are obtained compared to 0.1% with gas puff systems operating with higher peak currents.[4] The voltage pulse applied to the load by the Blumleins is highly dependent on the switch inductance. This is illustrated in Fig. 24 with the voltage estimates for two single Blumleins with 5-, 10-, and 15-nH combined switch inductance. The short-cir-

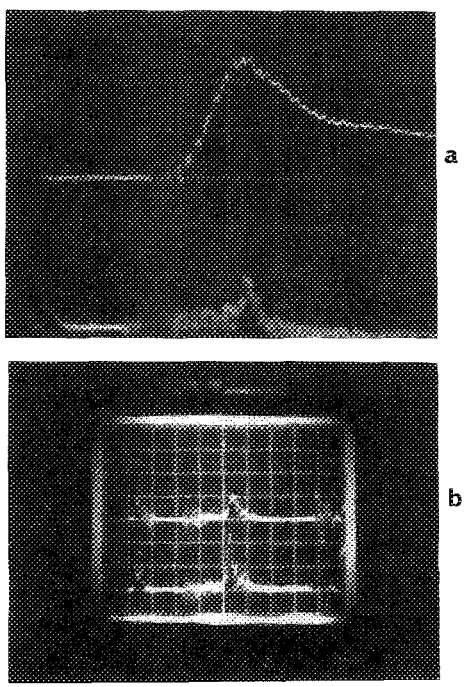

FIG. 23. Typical results with the dual double Blumleins and 25.4-μm annular puff with (a) current (100 kA/div, 200 ns/div), (b) p-i-n diode with 25-μm Be filter, (c) XRD with a saran filter (50 mV/div), and (d) XRD with Mylar filter (500 mV/div).

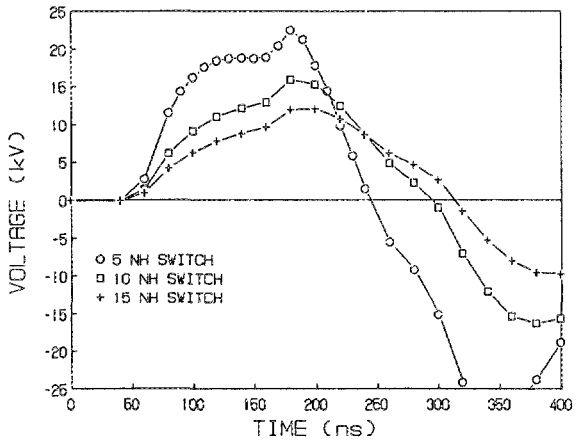

FIG. 24. Simulated load voltages for the dual single Blumlein configuration dc charged to 25 kV assuming 5-, 10-, and 15-nH switch inductance.

cuit current simulations indicate a 12-nH inductance for the high-voltage rail gap switches which are utilized. The voltage and current pulses and thus the energy coupling efficiency can be improved by using Blumlein switches which are better matched to the lower voltage requirements.

There has been no direct attempt to measure the liner formation parameters. Some relevant information can be inferred from the implosion experiments. A 9-μs minimum delay is required to obtain uniform breakdown of the annular liner. Shorter delays result in either arc formation or breakdown at the vacuum insulator interface. The minimum delay is consistent with the plasma transit time from the plenum to the opposing electrode assuming the sound velocity for a 3-eV plasma.

The liner mass coupled to the Z-pinch implosion is very independent on the diode structure. The plenum pressure and delay regime for optimum operation with the double Blumlein changed substantially when the screen in the ground electrode was modified to a coarse wire mesh as shown in Fig. 18. Both screens are 75% open with only the wire size and number varying. The exact reason for the slower mass accumulation with the coarse screen is not known. A possibility is that the coarser screen results in less resistance to the escape of the high-temperature gas injected into the electrode gap. As was noted earlier, the stagnation of the plasma flow does play an important role in the formation of sufficiently dense annular shells.

The delay interval between the discharge of the solenoid and Z-pinch currents is critical. The specific effects are illustrated with a sequence of shots using the triple Blumlein configuration, a fixed plenum pressure, and delays varying from 15–25 μs. The peak current, implosion time, and peak Mylar signal are given in Fig. 25. All parameters increase rapidly for the initial half of the interval with the mass coupled to the liner implosion increasing by 0.1 μg/μs. The accumulation process saturates in the latter half of the time interval as indicated by the constant implosion times and peak currents. The ring-down time for the solenoid capacitor is 20 μs, thus indicating the mass accumulation in the interelectrode gap is very dependent on the continued heating of the plasma in the plenum. The radiation output decreases with the longer delays with maximum emission obtained for the time delay interval at which the implosion time and peak current saturates. Possible reasons for the decrease are the expansion of the plasma liner with time as well as the decrease in preionization from the gas puff discharge.

The use of a coarse screen to extend electrode life with the double Blumlein configuration resulted in operation in a high plenum pressure long delay interval regime with minimum radiation output. The annular gap between the gas plenum and the main chamber was enlarged to 38 from 25 μm, thus increasing the initial cold flow rate for a given plenum pressure. With the larger gap, the optimum operating regime returned to the lower pressure shorter delay intervals required for high-power radiation signals. There is thus an upper limit for the plenum pressure for maximized mass injection into the plenum. For plenum pressures in the 8–10-Torr range, sufficient energy cannot be coupled to the plasma to give maximum pressure increases and thus a high mass injection rate. The enlargement of the annular gap does allow for pressure adjustment with higher initial gas flows. There is thus some flexibility in extending the system to produce higher mass liners. However, this approach is limited by the necessity of maintaining a pressure differential with the pressures in the main chamber below the level at which the electrical breakdown of the vacuum interface insulator becomes a problem and the plenum pressure is still above the Paschen minimum.

The triple Blumlein configuration should be able to implode 0.4–1.0-μg liners with peak currents in the 300–400-

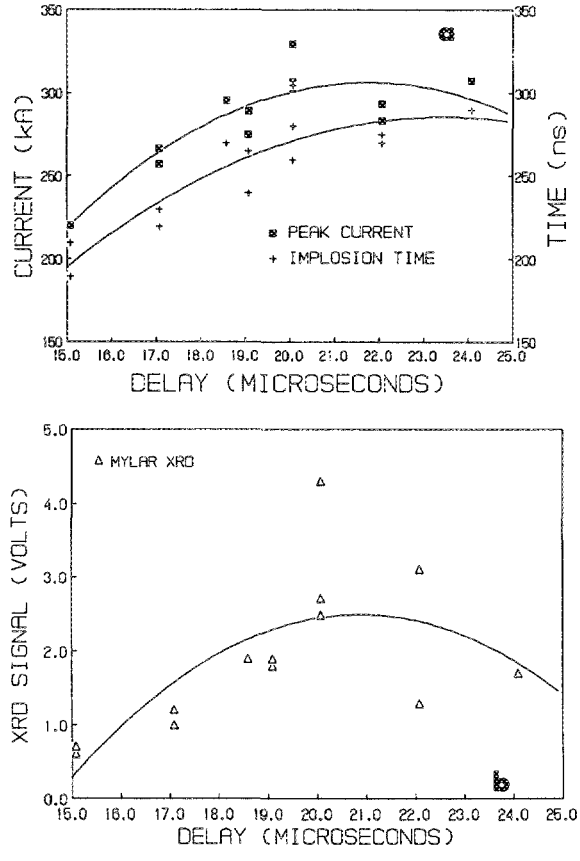

FIG. 25. Triple Blumlein results for a sequence of shots with the delay interval varied are shown for (a) the peak current and implosion time and (b) the Mylar filtered XRD output.

TABLE VI. Triple Blumlein implosion dynamics.

Mass (μg)	Implosion time (ns)	Peak current (kA)	Pinch current (kA)	Velocity (m/μs)	Kinetic energy (J)	Efficiency (%)
0.4	332	316.7	295.3	0.86	148.3	8.6
0.6	354	347.8	318.7	0.77	179.3	10.3
0.8	372	368.7	328.6	0.73	213.2	12.3
1.0	386	384.2	328.5	0.67	224.5	12.9

kA range (Table VI). However, experiments with the present 38.1-μm puff arrangement have only been able to couple up to 0.6 μg. Typical currents and radiation outputs are shown in Fig. 26. The simulation currents superimposed on the experimental traces are assuming 0.4- and 0.6-μg liner mass, respectively. The peak current is limited by the dynamic inductance with the lower mass loads. Peak radiation measurements with 5-J ultrasoft (Mylar/XRD) and 200-mJ soft x rays (12.5-μm Be/*p-i-n*) are obtained.

The soft x-ray emission was also measured using 50-μm Be and 25-μm Al filters coupled with *p-i-n* diodes with e^{-1} attenuation at 1.8 and 5.0 keV, respectively. The Al filter results indicate less than 20% of the radiation is in the higher energy range. The soft x-ray energy proportion in the higher energy range increases for short delay low-density implosions. The two Be filter results are comparable for longer delay intervals. Both signals increase for shorter delays with higher outputs obtained with the 12.5-μm filter. The lower density implosions also give an increase in the emission in the 0.9–1.8-keV range. Pinhole images show some radiation emission from the anode surface which increases with the lower density implosions. A small intense radiation point is also observed in the interelectrode region. Images superimposing 5–10 shots show minimum shot-to-shot variation in position. 0.5-mm pinholes with 1:1 magnification have been used. This suggests a <0.5-mm source diam including cumulative position scatter.

D. Capillaries

Experiments were also carried out with the capillary systems summarized in Table II. The cold flow conditions are comparable to the annular system (Figs. 4 and 5). The eight capillaries in parallel were not able to inject sufficient mass into the system. Also, with the concentration of the initial current, electrode erosion became a problem. The sixteen and thirty-two capillary systems were both able to produce liners with similar masses to the annular slit system with 240- and 320-kA peak currents obtained with the double and triple Blumlein systems, respectively. Comparable ultrasoft radiation output could be obtained. However, the soft x-ray emission is considerably lower with only narrow, 20–50-ns saran/XRD and Be/*p-i-n* signals produced. These signals are earlier than the ultrasoft emission rather than at the same time or slightly later, as found with the annulus. Also, the capillary system requires operation in a low-pressure long delay regime to obtain any soft x-ray output. The two systems thus have considerably different operating characteristics. The capillary system may require sufficient time for the plasma to expand and form a more uniform annular plasma ring rather than a series of plasma wires before a tight well-defined pinch can be produced.

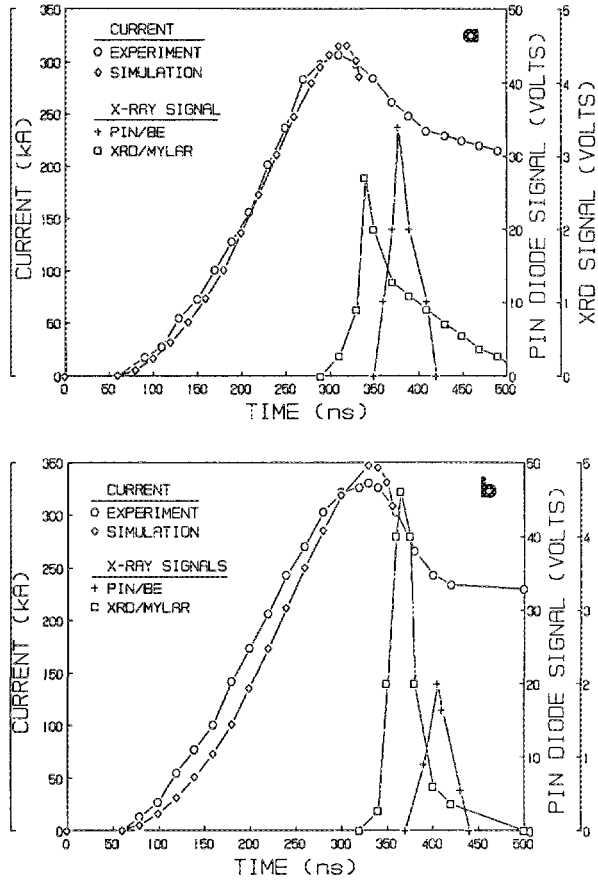

FIG. 26. The experimental and simulated currents, Mylar filtered XRD, and *p-i-n* diode with 12.5-μm Be filter are shown for the triple Blumlein configuration with (a) 18-μs and (b) 20-μs delay interval.

VIII. CONCLUSIONS

The solenoid gas puff system is a unique device for producing the initial annular loads for ultrafast *Z*-pinch implosions. In this device, the gas continuously flows into the chamber from a gas plenum with the annular plasma liner formed by increasing the mass flow rate for short time durations using a discharge in a single turn coil to heat the gas in the plenum. This approach only increases the gas flow rate through the narrow opening between the plenum and the *Z*-pinch electrodes, but does not increase the overall gas load significantly on the vacuum pumping system. The dead gas introduced into the chamber is minimized, and system repetition rate will now be dictated by thermal load problems on the main electrodes as well as the power supplies.

The annular loads produced by the solenoid gas puff system are already preionized by the current in the plenum. This has allowed the production of relatively low mass, low density, and large initial radius liners with uniform initial gap breakdown, which minimizes perturbations and thus minimizes instability growth under implosion.

Experiments have been carried out under a broad range of operating conditions and a variety of driver systems as well as puff geometry. These results coupled with the zero-dimensional model for the *Z*-pinch implosions have pro-

TABLE VII. X-ray emission.

Bank configuration	C (μF)	V (kV)	Bank energy (kJ)	Pinch current (kA)	Pinch time (ns)	X-ray emission 100–288 eV (J)	X-ray emission 1.5–2.8 keV (mJ)
Capacitor	5.6	30	2.5	175	400	3	10
Peaking	5.6 (8×0.22)	20	1.1	180	250	3	10
Blumlein	3.7	25	1.1	230	320	3	150
Blumlein	5.6	25	1.7	350	350	5	500

duced some understanding of the solenoid gas puff system and the relevant operating parameter. The more important results as well as limitations are briefly summarized:

(1) The inductive heating of the gas in the plenum with the solenoid current discharge does produce the expected factor of 10 increase in mass flow rate, if the plenum pressure is in the 1–5-Torr range. The energy coupling is not sufficient with the present arrangement for higher pressure regimes. A redesign of the solenoid current generator to optimize energy coupling to the plenum gas may allow for higher pressure operation.

(2) The solenoid gas puff arrangement has been able to couple large initial radius, low mass liners to the Z-pinch implosions. With the present arrangement, the mass accumulated is limited to the 0.1–0.5-μg range.

(3) The simulation results indicate high final implosion velocities can be achieved. The capacitor bank results indicate a minimum velocity in the 0.3–0.5-m/μs range is required to obtain measurable soft x-ray emission. The high velocity (0.5–1.0 m/μs) low-density implosions obtained with the Blumlein system coupled to the large initial radius system may result in poor thermalization of the kinetic energy and considerable hard x-ray emission due to electron effects in the gas and on the electrodes.

(4) Pinhole images indicate the predominate radiation source is localized to a small volume (<0.5 mm diam) including shot-to-shot variation.

(5) Implosions can be obtained using a capillary puff arrangement. A large number of apertures are required to minimize electrode effects by the localized current. The operating regime is different from that found with the annular system with long delays required to produce optimum emission. However, long delays tend to produce more diffuse pinches with minimum soft x-ray emission.

(6) The solenoid gas puff discharge gives a uniform preionization of the liner which helps produce a uniform breakdown with the Z-pinch current. The x-ray emission in the ultrasoft (150–288 eV) and soft x-ray (1.5–2.8 keV) regions is summarized in Table VII.

(7) The results with the solenoid gas puff system indicate that the I_m^4 scaling for the soft x-ray emission from krypton pinches can be extended to lower pinch currents. However, these results indicate that a minimum of 300-kA pinch current is required to give substantial soft x-ray emission. The energy coupling efficiency should also increase as the system is extended into the higher current regime.

(8) The dc charged Blumlein systems are able to efficiently drive high peak current pulses into both short-circuit and dynamic loads with the high dynamic impedance produced by the liner motion limiting the peak current in the latter case. The utilization of lower inductance switches could increase both the peak current and current rise time and result in improved energy coupling to the load.

The solenoid gas puff system is able to produce low mass liners formation for Z-pinch implosions. The system can in principle be extended to produce a repetitive x-ray source. However, the mass injected using only inductive heating is limited and restricts the system to large diameters. A new arrangement which will utilize electromagnetic forces as well as inductive heating is being tested as a means to further increase the mass injection rate, and thus obtain increased radiation output. The results with this new configuration will be reported in a subsequent paper.

[1] A. D. Wilson, SPIE J. **537**, 85 (1985).
[2] J. Lyman, Electronics, Dec. 2, 1984, p. 45; J. Lyman, Electronics, Oct. 7, 1985, p. 36.
[3] D. L. Spears and H. I. Smith, Electron. Lett. **8**, 102 (1972); D. L. Spears and H. I. Smith, Solid State Technol. **15**, 21 (1972).
[4] J. S. Pearlman and J. C. Riordan, SPIE J. **537**, 102 (1985).
[5] J. Pearlman and J. C. Riordan, J. Vac. Sci. Technol. **19**, 1190 (1981); J. Bailey, A. Ettinger, A. Fisher, and R. Feder, Appl. Phys. Lett. **40**, 33 (1982); G. Dahlbacka, S. M. Matthews, R. Stringfield, I. Roth, R. Cooper, B. Ecker, and H. M. Sze, in *Low Energy X-ray Diagnostics 1981*, edited by D. T. Atwood and B. L. Henke, AIP Conference Proceedings, No. 75, 1981; I. Okada, Y. Saitoh, S. Itabash, and H. Yoshihara, J. Vac. Sci. Technol. B **4**, 243 (1986).
[6] K. E. Liu, Ph.D. thesis, University of Houston, 1983; Y. Kato and S. H. Be, Appl. Phys. Lett. **48**, 686 (1986).
[7] K. S. Han, G. W. Lee, Y. K. Sohn, and J. H. Lee, Bull. Am. Phys. **31**, 1453 (1986).
[8] P. J. Turchi and W. L. Baker, J. Appl. Phys. **44**, 4936 (1973).
[9] C. Stallings, K. Neilson, and R. Schneider, Appl. Phys. Lett. **40**, 404 (1976).
[10] J. Shiloh, A. Fisher, and N. Rostoker, Phys. Rev. Lett. **40**, 515 (1978).
[11] B. Fay, in *Microcircuit Engineering*, edited by H. Ahmed and W. C. Nixon (Cambridge University Press, New York, 1980), p. 323.
[12] A. Ballantyne, H. Hyman, C. L. Dym, and R. Southworth, J. Appl. Phys. **58**, 4717 (1985).
[13] A. Heuberger, SPIE J. **448**, 8 (1983).
[14] A. Fisher, F. Mako, and J. Shiloh, Rev. Sci. Instrum. **49**, 872 (1978).
[15] E. Ruden, H. U. Rahman, A. Fisher, and N. Rostoker, J. Appl. Phys. **61**, 1311 (1987).
[16] R. P. Gupta, M. M. Kekez, J. H. W. Lau, and G. D. Lougheed, "Gas Discharge Derived Annular Plasma Pinch X-ray Source," Canadian and US patents, 1988 (unpublished).
[17] R. W. Carlson, in *Methods of Experimental Physics, Volume 14 Vacuum Physics and Technology*, edited by G. L. Weissler and R. W. Carlson (Academic, Toronto, 1979), p. 11.

[18]H. C. W. Beijerinck and N. F. Verster, Physica **111C**, 327 (1981).
[19]R. L. Summers, NASA Technical Note TND-5285 (unpublished).
[20]J. R. Woodworth and P. F. McKay, J. Appl. Phys. **58**, 3364 (1985).
[21]T. Sakurai and T. Watanabe, J. Appl. Phys. **59**, 4007 (1986).
[22]M. Vlach, University of Waterloo Technical Report No. UW EE 82-01, 1983 (unpublished).
[23]E. E. Bergmann, Appl. Phys. Lett. **28**, 84 (1975).
[24]Q. Johnson, A. C. Mitchell, and I. D. Smith, Rev. Sci. Instrum. **51**, 741 (1980); C. B. Collins, F. Davanloo, and T. S. Bowen, Rev. Sci. Instrum. **57**, 863 (1986).
[25]M. M. Kekez, R. P. Gupta, J. H. W. Lau, and G. D. Lougheed, in *Proceedings of 6th IEEE Pulsed Power Conference*, edited by B. H. Bernstein and P. J. Turchi (IEEE, New York, 1988), p. 178.
[26]I. Weinberg, Ph.D. thesis, University of California, Irvine, 1985.
[27]Model 40100 Rail Gap Switch, Maxwell Laboratories Inc., San Diego.
[28]Model 40151 100-kV HV Pulse Generator, Maxwell Laboratories Inc., San Diego.
[29]D. J. Rose and M. Clark, *Plasmas and Controlled Fusion* (MIT, Cambridge, MA, 1961).
[30]J. Katzenstein, J. Appl. Phys. **52**, 676 (1981).
[31]J. Apruzese and J. Davis, Naval Research Lab Memo No. NRL-MR-5406 (unpublished).
[32]J. H. Degnan, R. E. Reinovsky, D. L. Honea, and R. D. Bengston, J. Appl. Phys. **52**, 6550 (1981).
[33]Macor machineable glass ceramic, Corning Glass Works, Corning, NY.
[34]Model 31167, 0.22-μF, 100-kV *S*-type capacitor, Maxwell Laboratories Inc., San Diego, CA.
[35]W. L. Baker, M. C. Clark, J. H. Degnan, G. F. Kiuttu, C. R. McClenahan, and R. E. Reinovsky, J. Appl. Phys. **49**, 4694 (1978).
[36]100-PIN-125 soft x-ray diode, Quantrad Corporation, Torrance, CA.